ChemComm

Accepted Manuscript

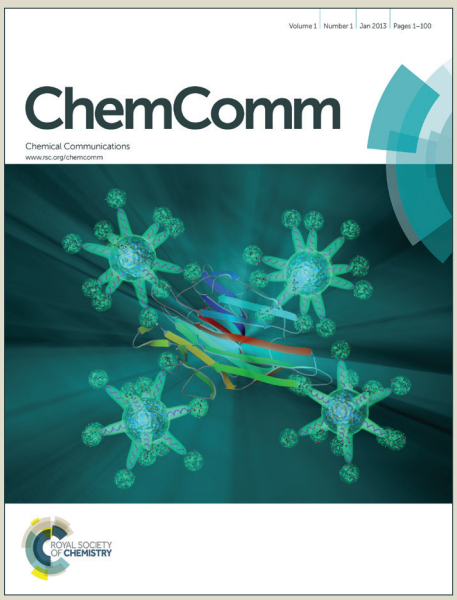

ROYAL SOCIETY OF CHEMISTRY

www.rsc.org/chemcomm

Journal Name

RSCPublishing

COMMUNICATION

A hybrid of holey graphene and Mn_3O_4 and its oxygen reduction reaction performance

Cite this: DOI: 10.1039/x0xx00000x

Xiaohui Lv, [a,c,‡] Wei Lv, [b,c,‡] Wei Wei, [a,c] Xiaoyu Zheng, [a,c] Chen Zhang, [a,c] Linjie Zhi [a, d,*] and Quan-Hong Yang [a,b,c,*]

Received ooth January 2012,
Accepted ooth January 2012

DOI: 10.1039/x0xx00000x

www.rsc.org/

A hybrid of holey graphene and Mn_3O_4 is prepared by a one-step process, in which the formation of holey structure is accompanied with Mn_3O_4 nanoparticles through a high temperature reaction between graphene oxide sheets and $KMnO_4$. Holey graphene and Mn_3O_4 collaboratively attributed to the enhanced catalytic activity and efficiency towards oxygen reduction reaction.

To meet the increasing demand for high performance energy devices, many advanced materials with high energy and power density have been developed. For instance, owing to its electrocatalytic mechanism, metal oxide is a very important electrocatalyst in the energy storage devices such as fuel cells and Li-O_2 batteries which have high energy density.[1] However, most of the oxides are always with lower electrocatalytic efficiency compared with noble metal catalysts due to their low conductivity and utilization, resulting in the limitation of their practical applications.[2] Various carbon matrixes have been used to disperse the oxides nanoparticles (NPs) to improve their performance, and graphene is considered to be a more promising matrix because of its high surface area and excellent conductivity.[3] However, the performance of the formed graphene-based hybrids is still hard to approach that of the noble metal-based catalysts due to their limited electrochemical activity.[4]

It has been widely accepted that the defects and edges on graphene can serve as active sites in electrocatalytic process,[5] and therefore introducing holey structure is an effective way to enhance the catalytic properties. It is suggested that combining oxide NPs with holey graphene sheet (HGS) should be more promising in the electrocatalytic applications. Regrettably, the enhancement of electrochemical activity of the holey structure on graphene sheets has rarely been reported. Various methods, such as photocatalytic oxidation, acid etching and template-directed chemical vapour deposition,[6] have been developed to prepare HGS, but most of these methods are complicated and of low yield. Moreover, following these methods, post deposition of oxide is needed to obtain HGS-oxide hybrids. Recently, metal ions have been proved to be able to break the C-C bond of graphene network under relatively mild condition,[7] providing a potential strategy to prepare HGS and indicating a possible way to have a hybrid structure of HGS and metal oxide in a one-step approach,

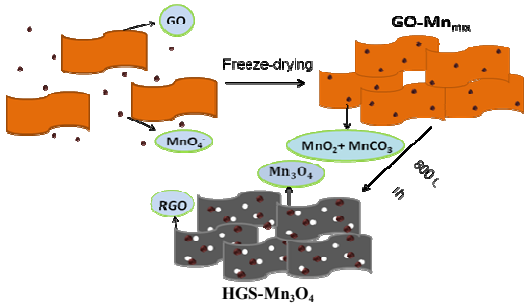

Scheme 1. Scheme of the one-step process for preparing a hybrid structure of HGS-Mn_3O_4.

in which metal salt simultaneously act as the reactants to introduce holey structure and precursor for oxide particles surrounding the holey structure.

In this communication, we realized the one-step preparation to obtain a hybrid of HGSs and Mn_3O_4 (HGS-Mn_3O_4). Uniformly distributed holes are identified on the graphene sheets, which were created by etching process of $KMnO_4$ towards graphene oxide (GO) at high temperature. $KMnO_4$ is then transformed into Mn_3O_4 particles surrounding the evenly distributed holes on the HGS. As is expected, the HGS-Mn_3O_4 hybrid shows high electrocatalytic activity toward the oxygen reduction reaction (ORR) in alkaline condition although Mn_3O_4 is always incorporated with N-doped carbons to reach high electrocatalytic performance.[4(a),8]. A high electron transfer number (n, ~3.69) is obtained for HGS-Mn_3O_4, which is much higher than that of non-holey graphene-Mn_3O_4 hybrid (n, ~3.18) and close to that of commercial Pt/C catalyst (n, ~3.98). More importantly, it shows higher onset potential and larger current density compared with the graphene-Mn_3O_4 hybrid, suggesting an enhanced electrocatalytic activity. The largely enhanced catalytic efficiency and activity should be ascribed to the synergistic effect of holey structure and Mn_3O_4, and the strong interaction between HGS and Mn_3O_4 inherited from the etching process.

The one-step preparation of the HGS-Mn_3O_4 hybrid is schematically shown in Scheme 1. In a typical experiment, $KMnO_4$ powder (45 mg) was added to the GO aqueous dispersion

(100 mL, 2 mg mL^{-1}) under stirring to obtain a uniform mixture. In such a process, the permanganate adsorbed on the GO surface and reacted with it forming the MnO_2 and $MnCO_3$, proved by the X-ray diffraction (XRD) pattern shown in Fig. S1(ESI†). The resident water was then removed by freeze-drying and the dried product (denoted GO-Mn_{mix}) was thermally treated under 800 °C for 1 h in Ar atmosphere to realize the reduction of GO and obtain the HGS-Mn_3O_4 hybrid. During the thermal treatment process, MnO_2 and $MnCO_3$ were decomposed and transformed into Mn_3O_4 and carbon atoms were etched to generate nanosized holes on the graphene sheets. The detailed preparation process is provided in the Supporting Information (ESI†). Moreover, the density of pores and the content of Mn_3O_4 can be easily tuned by control the amount of $KMnO_4$.

Fig. 1a shows the SEM image of the obtained HGS-Mn_3O_4 hybrid, from which uniformly distributed holes with the size of 40~100 nm can be observed on the graphene sheet. It is noted that a NP with the size ~50 nm always surrounding each generated hole, the TEM

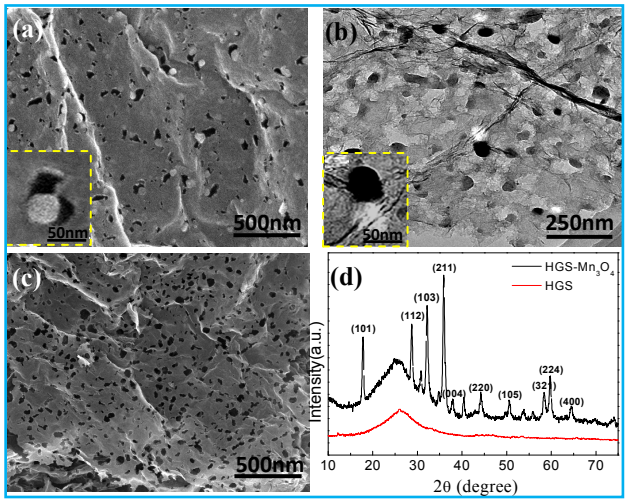

Fig. 1 (a) SEM image of HGS-Mn_3O_4, inset in (a) is the enlarged SEM image of single nanohole and adjacent Mn_3O_4 particle; (b) TEM image of HGS-Mn_3O_4, inset in (b) is the enlarged TEM image of single nanohole and adjacent Mn_3O_4 particle; (c) SEM image of HGS; (d) XRD pattern of HGS-Mn_3O_4 and HGS.

image (Fig. 1b) sees the similar finding, suggesting that these NPs may play a key role in the pore formation process. According to the XRD pattern of HGS-Mn_3O_4 (Fig. 1d), these particles are identified as Mn_3O_4, which can be inferred from the strong peaks indexed to a tetragonal spinel Mn_3O_4 with the space group of I41/amd (JCPDS card No.24-0734). The evolution process of the pore formation can be simply represented by the SEM images shown in Fig. S1 (ESI†). Although $KMnO_4$ first reacted with GO during the mixing process, no particles and pores can be found in the SEM image (Fig. S1a, ESI†), suggesting the formed MnO_2 and $MnCO_3$ are very small particles, which can be proved by the broadened peaks in XRD pattern (Fig. S1d, ESI†). After a thermal treatment under 300 °C, these manganic compounds were decomposed and transferred into Mn_3O_4, and uniformly distributed as small NPs but no holey structure can be observed on the graphene sheets (Fig. S1b, ESI†). When the temperature increased to 600 °C, these NPs grew larger (10~20 nm) and some holes can be observed (Fig. S1c, ESI†). It is noteworthy the appearing pores are almost of the same size with the NPs surrounding them, indicating the pores are formed by the etching of the Mn_3O_4 NPs. After the temperature increased to 800 °C for 1 h, uniformly distributed holes were generated with the slightly larger size than the NPs, as shown in Fig. 1a. When the thermal treatment time was prolonged to 3 h, the graphene sheets were greatly destroyed as shown in Fig. S2a (ESI†), and only very large Mn_3O_4 particles were left after 5 h (Fig. S2b, ESI†). These changes clearly show that the pores should be created by the etching of the Mn_3O_4 NPs and suggest the thermal treatment and the Mn_3O_4 NPs are both responsible for the pore formation. The holey graphene sheets (HGS) can be obtained by removing NPs from HGS-Mn_3O_4 through acid treatment, Fig. 1c and Fig. S5a show the porous surfaces of HGS, the successful removal of Mn_3O_4 can be proved by XRD pattern (Fig. 1d) and Raman spectra (Fig. S5b) of HGS.

The functional groups may also play a key role for the pore formation. When graphene replaces GO as the starting material, no holes are formed after the same preparation process (the obtained graphene-Mn_3O_4 is denoted as G-Mn_3O_4), as shown in Fig. S3a (ESI†). Although the formed NPs are also Mn_3O_4 (Fig. S3b, ESI†), the particle size is larger than the case of HGS-Mn_3O_4. The most obvious difference between GO and the graphene used here is that the functional groups of graphene are mostly removed, which can be proved by the X-ray photoelectron spectrometry (XPS) results shown in Fig. S4 (ESI†). Since the functional groups on GO plane are mainly hydroxyl and epoxy groups,[9] we believe these groups are responsible for the pore formation and they help prevent the growth of Mn_3O_4 NPs into large particles. As is widely reported, the epoxy bond on GO surface is easy to break forming lattice defects or chemical bonds with other compounds and has weaker reduction ability than hydroxyl groups.[10,11] $KMnO_4$ was reduced by hydroxyl groups forming MnO_2 and the formation of $MnCO_3$ may be derived from the reaction between $KMnO_4$ and epoxy groups, which help explain why some pores appear under relatively low temperature. The detailed mechanism study for the pore formation is underway.

Since the holes are formed by the reaction of Mn_3O_4 NPs with graphene, we believe that the strong interaction must exit between the formed Mn_3O_4 NPs and HGS. As shown in Fig. S5b (ESI†), the G-band in Raman spectra is right shifted for the HGS after removing the Mn_3O_4 NPs compared with the case of the HGS-Mn_3O_4 hybrid, indicative of the existence of strong interaction between Mn_3O_4 NPs and HGS.[12] Besides, a Mn-O-C bond can be found from the deconvoluted O1s XPS profile of HGS-Mn_3O_4 hybrid (Fig. S6b, ESI†), which does not exist in that of G-Mn_3O_4 hybrid (Fig. S7b, ESI†), also suggesting the interaction between the HGS and Mn_3O_4.

In order to investigate the electrocatalytic activity promoted by HGS, we compared the ORR performance of HGS-Mn_3O_4 hybrid and the reference samples in 0.1 M KOH solution. As the cyclic voltammetry (CV) profiles demonstrated in Fig. 2a, single cathodic reduction peaks can be detected in the O_2-saturated electrolyte for HGS-Mn_3O_4 and G-Mn_3O_4, the peak for HGS-Mn_3O_4 appears at around -0.19 V, apparently higher than that of G-Mn_3O_4 (-0.31 V), revealing that HGS-Mn_3O_4 has higher electrocatalytic activity. Rotating disk electrode (RDE) measurements were used to reveal the ORR kinetics of each sample. The linear-sweep voltammetry (LSV) curves of HGS-Mn_3O_4 at different rotation speeds are shown in Fig. 2b. Although the onset potential (-0.14 V) of HGS-Mn_3O_4 is lower than that of Pt/C (Fig. S8. ESI†), it is much higher than that of G-Mn_3O_4 (-0.22 V), HGS (-0.33 V) and Mn_3O_4 (-0.22 V), and the limiting diffusion current is also higher than that of else samples (Fig. S9-S12, ESI†), suggesting the enhancement of electrochemical activity. Its high electrocatalytic activity can also be demonstrated by the higher half-wave potential than those of G-Mn_3O_4 and Mn_3O_4 which are listed in Table S1 (ESI†). The calculated Koutecky-Levich (K-L) plots for HGS-Mn_3O_4 at the

potential of -0.35 ~ -0.5 V are shown in Fig. 2c. The electron transfer number estimated from the slope of K-L plot is 3.69 at -0.35 V, much higher than that of G-Mn_3O_4 (n=3.16) and close to

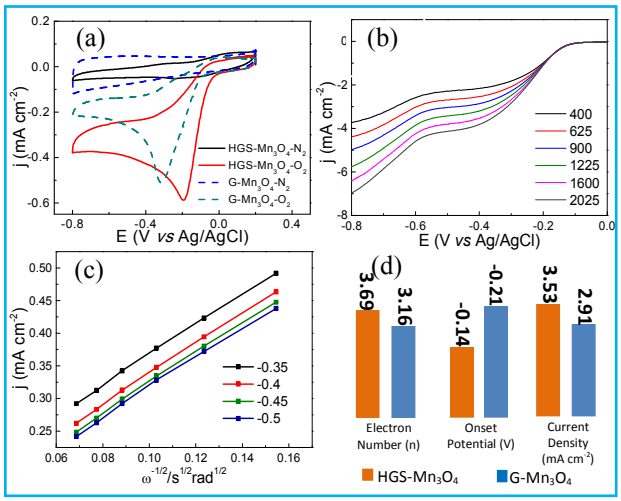

Fig. 2 (a) CV curves (scanning rate of 5 mV s^{-1}) of HGS-Mn_3O_4 and G-Mn_3O_4 in N_2 and O_2-saturated 0.1 M KOH solution; (b) LSVs (50 mV s^{-1}) at different rotating speeds on HGS-Mn_3O_4 in an O_2-saturated 0.1 M KOH solution. (c) Calculated K–L plots of HGS-Mn_3O_4. (d) Comparison of HGS-Mn_3O_4 and G-Mn_3O_4 on electron transfer numbers, onset-potential and current density at -0.4 V.

that of a commercial Pt/C catalyst (n=3.98), exhibiting a close to $4e^-$ process for ORR. The high performance of HGS-Mn_3O_4 should be ascribed to the interaction and synergic effects between the two components because much lower electron transfer number can be reached for HGS and Mn_3O_4 used alone (2.95 and 3.10 respectively). The electron transfer number increase with the increase of content of Mn_3O_4 in the hybrid (*e. g.* 12 wt % of Mn_3O_4, n=3.44, calculated by the K-L plots in Fig. S13, ESI†), but much higher Mn_3O_4 only result in slightly higher electron transfer number (*e. g.* 60 wt % of Mn_3O_4, n=3.81, calculated by the K-L plots in Fig. S14, ESI†) but lower onset potential (-0.18 V) and current density which does not favor to the electrocatalytic process. A diffusion control step at the potential about -0.6 V can be observed from the LSV curves under high rotation rate (Fig. 2b), suggesting the ORR does not follow a one-step 4-electron pathway and 2-electron transfer reduction also exists.[13] Above results also suggest that there are two kinds of ORR active sites in HGS-Mn_3O_4.[14] The high activity of the hybrid can also be proved by the Tafel plot (Fig S15, ESI†), which shows a slope (73 mV/decade) close to that of Pt/C (70 mV/decade) at low overpotential. However, much larger Tafel slope at high overpotential is observed for the HGS/Mn_3O_4 hybrid, indicating the first electron transfer for protonation of O_2 on the active sites is the rate-determining step.[1(a),15] Besides, this hybrid shows high durability than Pt/C after 2000th cycles with accelerated durability test, which can be seen from the Fig S16(ESI†). The comparison of electrocatalytic performance between HGS-Mn_3O_4 and G-Mn_3O_4 is presented in Fig. 2d, which clearly shows the great enhancement derived from the HGS since these two hybrids have the similar fractions of Mn_3O_4 (Fig. S17, ESI†). Two factors may be responsible for the apparently improved ORR activity. One is the largely increased defects and edges, which can be viewed as the active sites, along with the higher specific surface area of HGS-Mn_3O_4 hybrid (Fig. S18, ESI†), enhancing the adsorption of oxygen and making the oxygen get electrons easier during the electrochemical reaction. Another is the strong interaction between HGS and Mn_3O_4. As widely reported, the interaction between the catalysts and the carbon enhances the electron transfer process, and thus, promotes the catalytic activity of the catalyst NPs.[3,16] We are still making efforts to investigate the detailed mechanism for the electrocatalytic activity.

In summary, a HGS-Mn_3O_4 hybrid is prepared from GO and $KMnO_4$ by a simple one-step etching process. The hybridization of Mn_3O_4 with HGS, which has holey structure, results in a great enhancement of ORR performance of alone Mn_3O_4 and HGS. Also, due to more active sites and strong interaction between HGS and Mn_3O_4, HGS-Mn_3O_4 has a much better ORR performance than the hybrid of non-holey graphene and Mn_3O_4. This study not only provides a simple method for preparing a hybrid of holey graphene and oxide, but also, more importantly, indicates an effective strategy to design and prepare high performance catalysts.

We appreciate support from National Basic Research Program of China (2014CB932400), National Natural Science Foundation of China (Nos. 51372167 and 51302146), Shenzhen Basic Research Project (Nos. JC201104210152A and ZDSYS20140509172959981). We also thank the financial support from Guangdong Province Innovation R&D Team Plan (No. 2009010025).

Notes and references

[a] *Key Laboratory for Green Chemical Technology of Ministry of Education, School of Chemical Engineering and Technology, Tianjin University, Tianjin 300072, China; qhyangcn@tju.edu.cn.*
[b] *Engineering Laboratory for Functionalized Carbon Materials and Shenzhen Key Laboratory for Graphene-based Materials, Graduate School at Shenzhen, Tsinghua University, Shenzhen 518055, China; yang.quanhong@sz.tsinghua.edu.cn.*
[c] *Collaborative Innovation Center of Chemical Science and Engineering, Tianjin 300072, China .*
[d] *National Center for Nanoscience and Technology, Beijing, 100190, China; zhilj@nanoctr.cn*
† Electronic Supplementary Information (ESI) available: Details of the preparation and characterization results.. See DOI: 10.1039/b000000x/
‡ These authors are equal main contributors.

1. (a) J. B. Xu, P. Gao and T. S. Zhao, *Energy Environ. Sci.*, 2012, **5**, 5333; (b) J. Zhang, Y. B. Zhao, X. Zhao, Z. L. Liu and W. Chen, *Sci. Rep.*, 2014, **4**, 6005.
2. Y. Tan, C. Xu, G. Chen, X. Fang, N. Zheng and Q. Xie, *Adv. Funct. Mater.*, 2012, **22**, 4584.
3. Y. Y. Liang, Y. G. Li, H. L. Wang, J. G. Zhou, J. W, T. Regier and H. J. Dai, *Nat. Mater.*, 2011, **10**. 780.
4. (a) J. J. Duan, Y. Zheng, S. Chen, Y. H. Tang, M. Jaroniec and S. Z. Qiao, *Chem. Commun.*, 2013, **49**, 7705; (b) S. S. Li, H. P. Cong, P. Wang and S. H. Yu, *Nanoscale*, 2014, **6**, 7534.
5. Y. J. Gao, D. Ma, C. L. Wang, J. Guan, X. H Bao, *Chem. Commun.*, 2011, **47**, 2432.
6. (a) Y. W. Zhu, S. Murali, M. D. Stoller, K. J. Ganesh, W. W. Cai, P. J. Ferreira, A. Pirkle, R. M. Wallace, K. A. Cychosz, M. Thommes, D. Su, E. A. Stach and R. S. Ruoff, *Science*, 2011, **332**, 1537; (b) X. Zhao, C. M. Hayner, M. C. Kung and H. H. Kung, *ACS. Nano.*, 2011, **5**, 8739.
7. (a) X. Y. Xie, C. Zhang, M. B. Wu, Y. Tao, W. Lv and Q. H. Yang, *Chem. Commun.*, 2013, **49**, 11092; (b) Y. Zhao, C. G. Hu, L. Song, L. X. Wang, G. Q. Shi, L. M. Dai and L.Q. Qu, *Energy Environ. Sci.*, 2014, **7**, 1913.
8. (a) D. K. Huang, B. Y. Zhang, S. H. Li, M. K. Wang and Y. Shen, *ChemElectroChem*, 2014, **1**, 1531; (b) S. Bag, K. Roy, C. S. Gopinath and C. R. Raj, *ACS Appl. Mater. Interfaces,* 2014, **6**, 2692; (c) J. J. Duan, Y. Zheng, S. Chen, S. Dai and S. Z. Qiao, *Adv. Funct. Mater.*, 2014, **24**,

2072; (d) C. S. Sharmaa, R. Awasthia, R. N. Singha and A. S. K. Sinhab, *Electrochim. Acta,* 2014, **136**, 166.
9. D. R. Dreyer, S. Park, C. W. Bielawski and R. S. Ruoff, *Chem. Soc. Rev*., 2010, **39**, 228.
10. O. C. Compton, D. A. Dikin, K. W. Putz, L. C. Brinson, S. T. Nguyen, *Adv. Mater*., 2010, **22**, 892.
11. D. W. Wang, A. J. Du, E. Taran, G. Q. Lua and I. R. Gentle, *J. Mater. Chem*., **22**, 21085.
12. (a) A. Rao, P. Eklund, S. Bandow, A. Thess and R. E. Smalley, *Nature*, 1997, **388**, 257; (b) G. Zhou, D. W. Wang, L. C. Yin, N. Li, F. Li and H. M. Cheng, *ACS. Nano*., 2012, **6**, 3214.
13. Z. S. Wu, S. Yang, Y. Sun, K. Parvez, X. Feng, K. Mullen, *J. Am. Chem. Soc*., 2012, **134**, 9082
14. J. Sun, Y. H. Fang, Z. P. Liu, *Phys. Chem. Chem. Phys***.**, 2014, **16**, 13733.
15. FH. B. Lima, M. L. Calegaro, E. A. Ticianelli, *Electrochim., Acta,* 2007, **52**, 3732.
16. (a) R. Kitaura, N. Imazu, K. Kobayashi, H. Shinohara, Nano Lett., 2008, **8**, 693; (b) S. Guo, S. Dong, *Chem. Soc. Rev*., 2011, **40**, 2644.

